Med8, Med18, and Med20 subunits of the Mediator head domain are interdependent upon each other for folding and complex formation

David Adler[a], Hamidur Rahaman[b], Pernilla Wittung-Stafshede[b], and Stefan Björklund[a,1]

[a]Department of Medical Biochemistry and Biophysics and [b]Department of Chemistry, Umeå University, SE-901 87 Umeå, Sweden

We have studied folding and complex formation of the yeast Mediator head-module protein subunits Med8, Med18, and Med20. Using a combination of immunoprecipitation, far-UV circular dichroism, and fluorescence measurements on recombinantly expressed and denatured proteins that were allowed to renature separately or in different combinations, we found that Med8, Med18, and Med20 can fold in different ways to form both soluble monomeric proteins and different distinct subcomplexes. However, the concurrent presence of all three protein subunits during the renaturation process is required for proper folding and trimer complex formation.

assembly | protein folding | transcription

Unregulated, or basal, transcription of protein-encoding genes in eukaryotes requires RNA polymerase II (Pol II) and five general transcription factors (1). In addition, Mediator is a multisubunit complex that stimulates basal transcription and function as a central coregulatory complex to convey signals from promoter-bound transcriptional regulatory proteins (activators and repressors) to the general transcription machinery (2–4). Mediator was originally described in *Saccharomyces cerevisiae*, but has since been identified in a wide range of eukaryotes (5–13).

A combination of results in yeast using both electron microscopy (EM) and biochemical purification of Mediator from mutant strains lacking different subunits have revealed that Mediator can be divided in three modules termed "head," "middle," and "tail" (14–16). The tail module is primarily involved in interactions with transcriptional activator proteins, while the middle domain is composed of proteins important for negative regulation (17, 18). The head module is mainly composed of proteins encoded by so-called SRB genes, which were identified in a screen for suppressors of truncation mutants of the RNA Pol II C-terminal domain (19). Med8, Med18, and Med20, which are studied here, represent a submodule of the Mediator head domain. A fourth, more loosely associated domain is called the cyclin-C domain, which comprises the cyclin C, cdk8, Med12, and Med13 proteins. This module is present in a subpopulation of the Mediator and has a function in transcriptional repression by phosphorylating the Pol II C-terminal domain.

There are only a few reports on structures of Mediator proteins either in complex form or individually. One explanation for this lack of structure information is that Mediator proteins are inherently difficult to express as recombinant proteins in soluble form. As mentioned above, EM and image processing have been used to obtain lower-resolution structures of Mediator domains, Mediator alone, and in complex with RNA Pol II (14, 16, 20). In addition, some high-resolution structures of *S. cerevisiae* and *S. pombe* Mediator proteins from the head, head-middle, and cyclin-C domains have been reported (21–25). However, in all these cases it was necessary to use proteins that were truncated, had central domains deleted, or had been partially proteolyzed to remove potentially flexible domains to obtain crystals that diffracted at high resolution.

After polypeptide assembly on the ribosome, proteins generally fold into their functional three-dimensional structures, although some proteins are proposed to be, at least in part, intrinsically disordered in the cell. While there is extensive information about folding processes of monomeric proteins (26–28), less is known about folding of functional protein complexes involving several polypeptides. For such systems, the proteins may fold individually first and then assemble into the functional unit, or binding interactions take place in unfolded or partially folded states, which then facilitate correct folding and assembly of the complete complex. Examples of both scenarios have been described for various homo-oligomeric proteins (29–32). For large oligomeric complexes composed of a number of different proteins (such as the Mediator complex), the complexity of the involved folding and assembly steps rises dramatically, and structural changes in the preassembled complex may further regulate its function. The modular architecture of the Mediator complex has been observed by cryo EM to undergo dramatic conformational changes upon interactions with activators and RNAP II. In analogy to many regulatory and transcriptional proteins, intrinsically disordered regions have been found in Mediator proteins using computer algorithms. Such regions are proposed to facilitate regulatory structural changes and to transmit transcriptional signals through Mediator to the general transcription machinery (33).

To study protein folding and conformation in vitro, purified proteins may be subjected to spectroscopic methods in combination with chemical or thermal perturbations to induce unfolding. Far-UV circular dichroism (CD) reports on the secondary structure content because α-helices, β-sheets, and random coil structures have distinct spectral appearances (34). Fluorescence is another tool that is often used to assess the environment of tryptophans in proteins: exposed tryptophans, such as in unfolded polypeptides, emit at higher wavelengths than tryptophans buried in the core of a folded protein.

Here we report on the folding and assembly process of the *S. cerevisiae* Med8-Med18-Med20 trimer from the head domain of the Mediator complex. We have used urea-denaturation followed by dialysis to buffer lacking urea to study the folding process and assembly of the three proteins using a combination of biochemical and biophysical methods. Our results indicate interdependence between all three proteins during the folding/
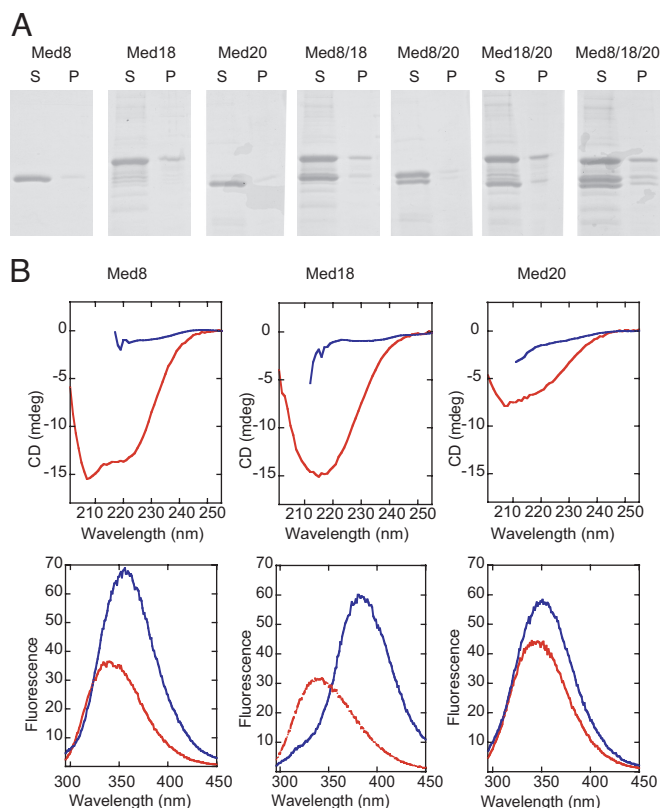
A

B

Fig. 1. Refolding of Med8, Med18, and Med20 as individual protein in the three possible dimer forms and in the trimer form by dialysis of each protein sample from 8 M to 0 M urea. (*A*) Approximately 30 mM of the indicated purified protein were used for each experiment. (*B*) Far-UV CD spectra (*Top*) and tryptophan emission (excitation at 285 nm) (*Bottom*) of individual proteins Med8, Med18, and Med20, each normalized to 5 μM protein concentration (20 °C) in buffer (*red*) and in 8 M urea (*blue*). The larger negative CD intensity for Med18 over Med20 is reasonable with respect to the molecular weight difference (34 kDa vs. 23 kDa).

assembly process, a finding that adds an important dynamic dimension to the previously reported high-resolution structures of the Med8-Med18-Med20 trimer complex.

Results

Denaturation of Med8, Med18, and Med20 in 8 M Urea Followed by Renaturation of Each Protein Individually and in Different Combinations. The three Mediator head-module proteins Med8, Med18, and Med20 were expressed individually as recombinant proteins in *Escherichia coli*. After disrupting the cells, we found that all three proteins were present in the insoluble protein fraction, thus indicating that they were improperly folded. In an attempt to obtain soluble proteins, we dissolved the insoluble protein fractions in a denaturing buffer containing 8 M urea. The proteins were then purified under denaturing conditions, as described in *Materials and Methods*. Each protein sample was then dialyzed over night into buffer lacking urea. Fig. 1*A* shows that all proteins, either individually or in the different combinations, become mostly soluble after denaturation/renaturation. To determine the structural states of the proteins, we recorded far-UV CD and fluorescence spectra for the individual proteins before (in 8 M urea) and after (in 0 M urea) renaturation (Fig. 1*B*). The data in Fig. 1*B* show that each protein in 0 M urea has a distinct CD signal in the far-UV range (200–220 nm) that is different from the unfolded-like signals found in 8 M urea. The CD signal for Med8 in buffer has negative peaks at 208 and 222 nm, in agreement with presence of α-helix, whereas the signal for

Table 1. Secondary structure predictions

Protein	α-helix (%)	β-strand (%)	Random coil and turns (%)
Med8	41 ± 5	17 ± 5	42 ± 5
Med18	11 ± 5	30 ± 5	59 ± 5
Med20	12 ± 5	31 ± 5	56 ± 5
Med8 + Med18	5 ± 5	38 ± 5	56 ± 5
Med18 + Med20	6 ± 5	37 ± 5	56 ± 5
Med8 + Med18 + Med20	17 ± 5	32 ± 5	54 ± 5

Predictions were made using the CDSSTR algorithm in Dichroweb (48, 49) that are based on the far-UV CD spectra (shown in Figs. 1*B* and 3) for individual Med proteins and dialyzed mixtures of two or three proteins (0 M urea). Output values for random coil and turn structures are merged. Errors in the values represent the effects of protein concentration variations (± 10%).

Med18 has one broad, negative peak at 215 nm, in accord with β-sheet: the CD of Med20 seems to be a combination of both secondary structures. Moreover, the emission from the Trp residues is shifted to lower wavelengths in buffer conditions (maximum, around 335 nm) as compared to in 8 M urea (maximum at 350 nm or higher) for all three proteins. The CD and fluorescence data demonstrates that each Mediator protein becomes folded upon dialysis from 8 M urea to buffer. The far-UV CD spectra in buffer were used to estimate the secondary structure content using the CDSSTR algorithm. It emerges from the values obtained (Table 1) that Med8 has about 40% α-helix, 15% β-sheet, and the rest is turns and random coil. The Med18 and Med20 structure both have more β-sheet structure (about 30% in each protein) and less helix structure (about 10% in each protein) as compared to Med8. The secondary structure content of Med18 and Med20 is in agreement with what is reported in the crystal structure (25). No structural data are reported for Med8, except for the helical 20-aa long C-terminal segment that is included in the Med18-Med20 crystal structure.

Interactions Between Individually Renatured Med8, Med18, and Med20 Proteins. We next studied if the Med8, Med18, and Med20 proteins can interact to form complexes when they have been renatured and folded as individual proteins. Med8, Med18, and Med20 were denatured in 8 M urea, dialyzed individually to buffer lacking urea, and then mixed in equimolar ratios in all different dimer combinations, as well as all three proteins together. Interactions were first studied by collecting far-UV CD spectra on the different mixtures. While mixtures of Med8-Med18, Med8-Med20, and Med8-Med18-Med20 initially exhibited CD spectra that matched that of the sum of the individual proteins, the Med18-Med20 mixture adopted a CD signal that was distinctly different from the individual components, with the negative maximum shifted to about 220 nm. However, with time all these protein mixtures appeared to aggregate, precluding further characterization. We also looked for interaction between the individually folded proteins using immunoprecipation, but we were unable to detect any interactions between Med8, Med18, and Med20 in any of the possible combinations of the proteins two-and-two or all three together (Fig. S1).

Renaturation of Med8, Med18, and Med20 in Different Combinations. The results presented above indicate that the Med8, Med18, and Med20 proteins require the presence of each other during the folding process to adopt conformations that allow functional interactions between the proteins. We therefore mixed the Med8, Med18, and Med20 proteins in all three possible dimer combinations and also mixed all three proteins together in 8 M urea, followed by dialysis to buffer lacking urea. Interactions between proteins were analyzed by immunoprecipitation using anti-Med8 antibodies or anti-Med20 antibodies. We found that
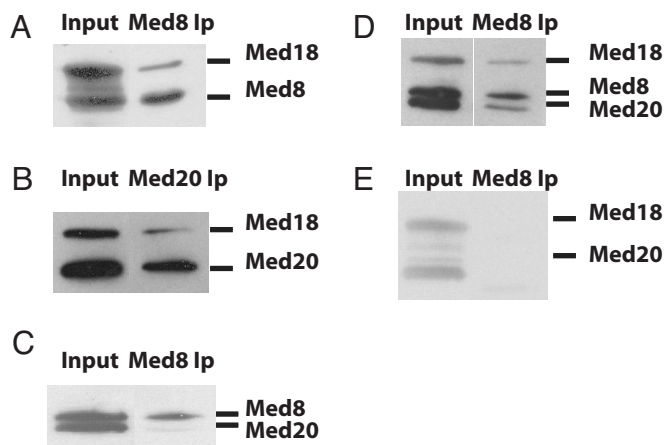
Fig. 3. Far-UV CD spectra of dialyzed Mediator protein combinations (*red*) at 20 °C. (*A*) Med8 and Med18. (*B*) Med8 and Med20. (*C*) Med18 and Med20. (*D*) Med8, Med18, and Med20. The expected CD signals based on the theoretical sum of the individual protein signals are also shown (*blue*).

Fig. 2. Interaction between Med8, Med18, and Med20 after renaturation in different combinations. In (*A*) through (*E*), lane 1 represents purified, recombinant histidine-tagged proteins expressed in *E. coli* purified under denaturing conditions (8 M urea) and then dialyzed to buffer lacking urea. In (*A*) and (*C*) to (*E*) lane 2 represents proteins that coimmunoprecipitate with anti-Med8 antibodies. In (*B*) lane 2 represents proteins that coimmunoprecipitate with Med20 antibodies. (*A*) Med8-Med18, (*B* and *E*) Med18-Med20, (*C*) Med8-Med20, and (*D*) Med18-Med8-Med20. Proteins were separated on 12% SDS/PAGE, transferred to PVDF membranes and blotted with anti-6× his-antibodies. Input lanes contain 10% of the amount of proteins used for the immunoprecipitations. The identity of different proteins is indicated to the right in each figure.

Med8-Med18 (Fig. 2*A*) and Med18-Med20 (Fig. 2*B*) form dimers when they are renatured together. However, Med8 and Med20 do not interact (Fig. 2*C*). These results are in agreement with the crystal structure results reported by Larivière et al. (25), who found that the Med18-Med20 complex has a very extended heterodimer interface (3,900 Å² buried surface area) and that the C-terminal 20 aa of Med8 interact with Med18, but not with Med20. Finally, we also found that all three proteins can be coimmunoprecipitated with anti-Med8 antibodies when they are renatured together (Fig. 2*D*). Because we had already shown that Med18 and Med20 form a dimer when renatured together, it is also important to notice that the coimmunoprecipitation of all three proteins with the anti-Med8 antibodies is dependent on the presence of Med8, and not because of nonspecific interaction between the Med18-Med20 dimer and the anti-Med8 beads (Fig. 2*E*).

To assess the secondary-structure content in the dialyzed mixtures of proteins, we probed the far-UV CD spectra of the Med8-Med18, Med8-Med20, Med18-Med20, and Med8-Med18-Med20 mixtures after they had been renatured together. In Fig. 3, we show the observed CD signal of the mixtures together with the expected signal that is based on the sum of the spectra for individual proteins (from Fig. 1*B*) and thus involves no conformational changes. Because there are protein concentration differences between the different protein samples, only CD spectral shape changes and not intensity changes should be interpreted. The experimental data shows that the Med8-Med18 as well as the Med18-Med20 mixtures, that both formed complexes in the immunoprecipitation experiments (see Fig. 2 *A* and *B*), adopt CD signals distinctly different in shape from that of the sum of the individual protein components. Specifically, the negative CD-peak maximum is found to shift from about 215 to 220 nm in these mixtures. CD spectra with negative maxima at 220 nm often correspond to protein structures containing β-sheet and β-turns (34). This observation implies that there are secondary structure changes upon formation of these dimers, as compared to the secondary structure found in the individual proteins. In accord, secondary structure analysis of the Med8-Med18 and Med18-Med20 CD spectra using the CDSSTR
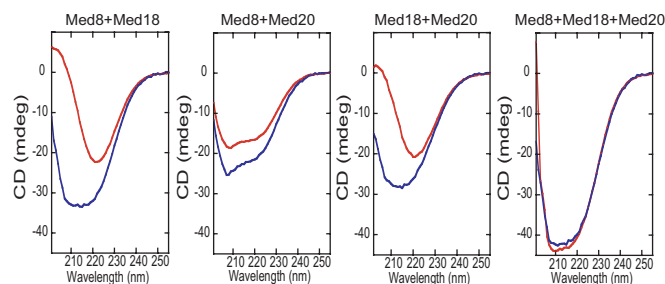
algorithm (see Table 1) suggests that both complexes contain more β-sheet (about 40%) and less α-helix (5%) than the individual proteins. In contrast, the combination of all three proteins, resulting in a trimer based on our immunoprecipitation data, exhibits a CD spectrum that matches the sum of the individual protein components in terms of shape, indicating no major structural changes upon assembly. The Med8-Med20 mixture did not result in a complex according to our immunoprecipitation experiment and, in agreement with this, the observed CD signal of this mixture is identical in shape to that of the sum of the individually dialyzed proteins.

Interactions Between the Med8-Med18 Dimer and Med20 Monomer and Between the Med18-Med20 Dimer and the Med8 Monomer. The results presented so far indicate that the Med8, Med18, and Med20 proteins are dependent upon each other for proper folding and trimer assembly. Nonetheless, we can show by immunoprecipitation that Med8-Med18 and Med18-Med20 form dimers when they are folded together. In addition, our CD spectra of Med8-Med18 and Med18-Med20 that have been renatured together indicate dimer formation, as they differ from the sum of the individually folded monomers in terms of shape. This suggests that formation of a functional Med8-Med18-Med20 trimer could be formed either by initial formation of a Med8-Med18 dimer to which a Med20 monomer could be added, or by initial formation of a Med18-Med20 dimer that can bind to a separately folded Med8 monomer. The results were also initially as expected, as it is reasonable that interaction between two proteins induces changes in their secondary structures. However, the results pose a conundrum because we also found that Med8, Med18, and Med20 form a trimer when folded together; however, in contrast to the Med8-Med18 and Med18-Med20 dimers, the Med8-Med18-Med20 trimer shows a CD spectrum that is the sum of the individually folded monomers. It is in this respect important to notice that even if the sum of distributions in different secondary structures for the individual subunits adds up to the distribution in different secondary structures of the entire trimer, it does not mean that the structural details of the subunits are identical when they are separate, compared to when they are in complex. To study if the Med8-Med18 and Med18-Med20 dimers represent productive complexes in the pathway of Mediator complex formation, we performed experiments where the two dimers after renaturation together were incubated with the third protein renatured by itself. Surprisingly, we found that neither of the dimers provide a base for trimer formation (Fig. 4 *A* and *B*), thus indicating that all three proteins need to be present together during the folding process. This further implies that the structurally different Med8-Med18 and Med18-Med20 dimers are not productive complexes in the pathway of Mediator assembly, but instead may represent misfolded species. An alternative explanation could be
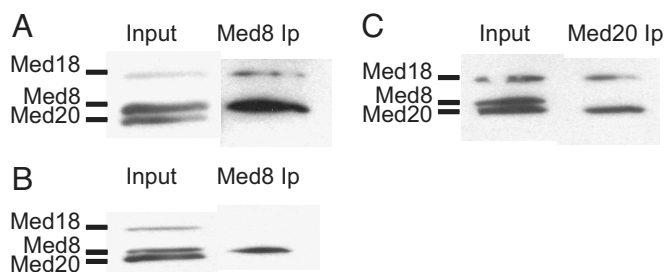
Fig. 4. Attempts to form Med8-Med18-Med20 trimers by mixing refolded dimers with refolded monomers. (*A*) Refolded Med8-Med18 dimer was mixed with Med20 that had been refolded by itself and then immunoprecipitated with anti-Med8 antibodies. (*B*) Refolded Med18-Med20 dimer was mixed with Med8 that had been refolded by itself and then immunoprecipitated with anti-Med8 antibodies. (*C*) As described in (*B*), but the proteins were immunoprecipitated with anti-Med20 antibodies. Proteins were separated on 12% SDS/PAGE, transferred to PVDF membranes and blotted with anti-6× his-antibodies. Input lanes contain 10% of the amount of proteins used for the immunoprecipitations. The identity of different proteins is indicated to the right in each figure.

that the Med8-Med18 and Med18-Med20 dimers are folded properly, but that the Med20 and Med8 monomers are misfolded. However, our biophysical data are more compatible with the first alternative.

Analysis of Med8. Med8 has been proposed to be a multidomain protein composed of an N-terminal helical domain followed by a flexible linker and, finally, a C-terminal helix that interacts with Med18 (25), although no structure has been reported. Our secondary structure estimates support the presence of a large amount of helix in Med8 (see Table 1). To investigate the structural integrity of Med8, urea-induced unfolding at 20 °C was probed by CD and fluorescence (Fig. S2). The unfolding reaction was found to be reversible (in accord with the ability to dialyze the protein from 8 M to buffer) and the transition, regardless of detection method, was broad with a midpoint at 3.5 M urea. Two-state fits to the data gave a folded-state stability in buffer of 10 to 15 kJ/mol, which is a very low value for a protein of this size. The low chemical stability and broad nature of the chemical perturbations are compatible with both a multidomain arrangement and the presence of disordered segments in the folded structure, as has been suggested (25).

Discussion
Most studies of the folding pathways for proteins have focused on monomeric proteins. These studies have aimed at revealing a protein-folding code where the primary structure contains the information for the pathway from the unfolded, random coil ensemble of states to the productive three-dimensional protein structures. Typically, small single-domain proteins show folding kinetics that are best described by a two-state mechanism (26, 35). However, multidomain monomeric proteins show more complex folding pathways that require both interdomain and intradomain interactions (36).

Folding of proteins that constitute complexes of different multidomain subunits have been studied in several different model systems. Two of the best-studied examples are the ribosome and the spliceosome complexes (37). Many studies suggest roles for chaperones and RNA helicases in ribosome assembly, but there are also reports suggesting that the basic assembly process is encoded in the RNA sequences and can occur spontaneously (38). Interestingly, both ribosome and spliceosome assembly is suggested to occur through the formation of subcomplexes, thus reducing the complexity of the complex formation (37).

The ribosome and the spliceosome differ from Mediator in that they are composed of both proteins and RNA. A more closely related example for assembly of a complex purely composed of proteins is therefore the nucleosome, which is composed of 147 bp of DNA wrapped nearly two turns around a protein core composed of four homodimers of each of the histone H2A, H2B, H3, and H4 proteins (39, 40). Nucleosome assembly is closely coupled to DNA replication in the S phase of the cell cycle. This occurs by random segregation of the existing histones onto the newly replicated DNA (41). The remaining nucleosomes are then synthesized and assembled in a highly ordered process. First, two heterodimers of histone H3/H4 are placed onto the DNA and then two dimers of H2A and H2B are recruited to the same site to form a histone octamer (42). This process requires chaperones, which are thought to mask the positive charge of histones to prevent nonspecific DNA-binding.

Nucleosome assembly is dependent on the histone fold, a dimerization motif that initially was characterized in heterodimers of the (H3–H4)$_2$ tetramer and the H2A–H2B heterodimer (40, 43). Histone folds are also found in several important protein–DNA complexes, such as the TATA-binding protein-associated factors complex (44, 45). Most histone-fold domains are insoluble when expressed in *E. coli* in the absence of their heterodimeric partners, most probably because the large hydrophobic surfaces that are hidden in the heterodimers (46, 47).

The results for the histone-fold proteins are similar to what we find when we express the Med8, Med18, and Med20 proteins individually in *E. coli*. We show that it is possible to obtain soluble Med8, Med18, and Med20 proteins by denaturation in 8 M urea followed by slow dialysis/renaturation to buffer lacking urea. However, these monomers cannot form a dimeric or trimeric complex when mixed together (see Fig. S1). Our CD spectra of these mixtures of individually renatured proteins initially indicated a change in secondary structure after mixing of Med18 and Med20, but with time all of these protein mixtures appeared to aggregate, which made further studies impossible. In contrast, we do find that Med8-Med18 and Med18-Med20 can form dimers when they are mixed in 8 M urea and then dialyzed together, but these dimers are improperly folded because they are unable to form a trimer when mixed with the missing subunit, which is renatured by itself. Instead, our results obtained by both CD measurements and immunoprecipitations show that a complete trimer of Med8, Med18, and Med20 can only form when they are allowed to fold in the presence of each other. Our results therefore suggest that complexes of Med8, Med18, and Med20 that are formed in a different way represent misfolded complexes. For proper trimer assembly, it appears that interactions before or during folding of the three polypeptides are necessary.

The notion that the Med18 polypeptide is prone to conformational changes may be consistent with differences in the crystal structures of Med18 from *Schizosaccharomyces pombe* (in complex with the *S. pombe* Med8C) and *S. cerevisiae* Med18 (in complex with Med8C and Med20). Specifically, two peptide regions in the *S. cerevisiae* Med18 seem to "grab" Med20, while this is not the case for *S. pombe* Med18 (where no Med20 is included) (23). Furthermore, the reported secondary structure contents based on the crystal structures of the two Med18 proteins differ: the *S. pombe* Med18 has 23% helix and 41% sheet, whereas *S. cerevisiae* Med18 has 22% helix but only 28% sheet.

Based on the results presented here, we suggest a model for proper folding and assembly of the trimeric Med8, Med18, and Med20 subcomplex of the mediator head domain (Fig. 5). We propose that proper assembly of a Med8-Med18-Med20 complex composed of full-length proteins requires that folding of the proteins occur in the presence of all three proteins. This finding, which is reminiscent of the assembly of complexes that comprise proteins with histone folds, indicates that in vivo assembly of
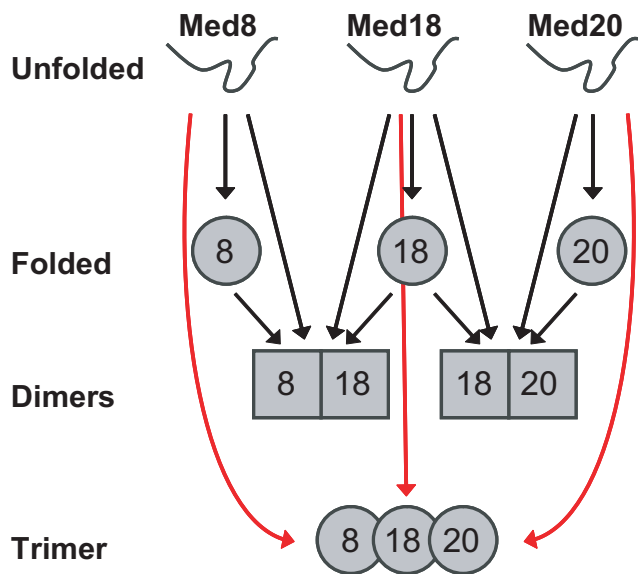
BIOCHEMISTRY

Fig. 5. Proposed model for the assembly of a functional Med8-Med18-Med20 trimer. Black arrows indicate folding pathways that lead to improperly folded protein monomers or protein dimers. Red arrows indicate the folding process that leads to a properly folded Med8-Med18-Med20 trimer.

Mediator requires specific chaperones or the general protein-folding chaperone/chaperonin systems.

Materials and Methods

Expression and Purification of His-tagged Med8, Med18, and Med20 Proteins from *E. coli*. The coding sequences of Med8, Med18, and Med20 were amplified from *S. cerevisiae* genomic DNA by PCR using the following oligonucleotides, Med8f (**CACC**ATGTCACAATCTACTGCATCA), Med8r (TCAATTACTAGATGATGTTGAAGT), Med18f (**CACC**ATGGTTCAGCAACTAAGCCT), Med18r (TTATATTAGAATATTTCCAT), Med20f (**CACC**ATGGGAAAATCAGCCGTTAT), Med20r (TCACAGCTCCAGAGCAC). The nucleotides in bold are included for in-frame cloning, such that the resulting PCR products when cloned into pET151 expression vector encodes for N-terminally 6× his-tagged proteins. The expression vectors were made using the Champion pET151 Directional TOPO Expression kit (Invitrogen) according to the manufacturer's instructions. The 6× his-tagged constructs were transformed into the *E. coli* strain BL21 Star (DE3). Two-liter cultures were grown at 37 °C to OD$_{600}$ ≈ 0.5 to 0.6. Protein expression was induced by addition of IPTG to a final concentration of 1 mM. The cultures were then grown at 37 °C for an additional 2 h. Cells were harvested by centrifugation and the resulting pellets were resuspended in 25-ml Lysis buffer (20 mM Tris-Ac pH 7.8, 20 mM Imidazole pH 8.0, 600 mM potassium acetate, 1 mM DTT, and protease inhibitors) and cells were lysed using CelLytic Express according to the manufacturers protocol (Sigma). The suspensions were rotated at room temperature for 15 min and then centrifuged at 33,000 × *g* for 10 min at 4 °C. The pellets were then resuspended in 11-ml denaturing B buffer (100 mM NaH$_2$PO$_4$, 10 mM Tris-Cl, 8 M urea, pH 8.0) and rotated at room temperature for 1 h followed by centrifugation at 14,000 × *g* for 10 min at 20 °C. The resulting supernatants containing denatured 6× his-tagged proteins were bound to 1-ml Ni Sepharose 6 Fast Flow (GE Healthcare) in PolyPrep Chromatography columns (Bio-Rad) by rotation at room temperature for 1 h. For purification of Med8 and Med20, the beads were first washed with 5-ml buffer B (100 mM NaH$_2$PO$_4$, 10 mM Tris-Cl, 8 M urea, pH 8.0) and the protein-bound beads were then washed with 5-ml buffer C (same as buffer B, pH 6.8) and then with 5-ml buffer D (same as buffer B, pH 5.9). Finally, the 6× his-tagged Med8 and Med20 were eluted by 5-ml buffer E (same as buffer B, pH 4.5). For purification of Med18, protein-bound beads were first washed with 5-ml buffer B (100 mM NaH$_2$PO$_4$, 10 mM Tris-Cl, 8 M

urea, pH 8.0) followed by washing with 5-ml buffer containing 100 mM NaH$_2$PO$_4$, 10 mM Tris-Cl, 8 M urea, and 125 mM Imidazole, pH 7.5. The 6× his-tagged Med18 was then eluted with buffer containing 100 mM NaH$_2$PO$_4$, 10 mM Tris-Cl, 8 M urea, and 250 mM imidazole, pH 7.5.

Dialysis of His-Tagged Med8, Med18, and Med20. The protein concentrations of the eluted Med8, Med18, and Med20 were determined to be 1.7 mg/ml, 0.65 mg/ml, and 0.36 mg/ml, respectively. Seven tubes containing the following combinations of proteins, Med18, Med20, Med8, Med18-Med20, Med8-Med18, Med8-Med20 and Med8-Med18-Med20, were set up for dialysis. For each dialysis experiment, 30.6 μg from the purified Med8 fraction, 140.4 μg from the purified Med18 fraction, and 38.9 μg of the Med20 fraction was mixed in a total volume of 342 μl of buffer D. These amounts from each fraction were determined by quantification of Coomassie-stained SDS/PAGE to result in addition of equimolar amounts of each protein in the dialysis step. Each protein mixture was dialyzed against 2× 300-ml dialysis buffer containing 100 mM NaH$_2$PO$_4$, 10 mM Tris-Cl, 1 mM DTT, pH 7.5 using Spectra/por Dialysis membranes (MWCO:12–14000, Spectrum Laboratories, Inc.) overnight at 4 °C. The mixtures were then centrifuged at 20,800 × *g* for 10 min at + 4 °C and the supernatants were analyzed for soluble proteins using SDS/PAGE followed by Coomassie staining.

Coimmunoprecipitations. Forty microliter fractions of the dialyzed supernatants of Med8-Med18, Med8-Med20, and Med8-Med18-Med20, were precleared with 50 μl of 50% protein A agarose beads (Sigma-Aldrich) by rotation at 4 °C for 2 h. An additional set of tubes containing 50 μl of Protein A agarose beads (Sigma-Aldrich), 10 μl of Med8 antibodies, and 30 μl of dialysis buffer were incubated by rotation at 4 °C for 2 h. Both set of tubes were centrifuged at 2,000 × *g* for 2 min and the precleared supernatants were then added to the Med8-bound protein A agarose beads. The samples were then incubated by rotation for 2 h at 4 °C, collected by centrifugation at 2,000 × *g* for 2 min, and then washed three times with 200-μl dialysis buffer. Detection of the proteins bound to the beads was then carried out using SDS/PAGE followed by Western blotting using anti-his antibodies (Sigma). For coimmunoprecipitations of dialyzed Med8-Med18 plus Med20 and Med18-Med20 plus Med8, the immunoprecipitation experiments were performed exactly as described above, with the exception that Med20 and Med8 were dialyzed individually then mixed with Med8-Med18 and Med18-Med20, respectively, before immunoprecipitation. The coimmunoprecipitation experiments of dialyzed Med18-Med20 plus Med 8 was performed exactly as described in the previous section, with the exceptions that Med8 was dialyzed individually then mixed with Med18-Med20 before the immunoprecipitation with anti-Med20 antibodies bound to the protein-A agarose beads.

CD and Fluorescence Measurements. The concentration of individually dialyzed Mediator proteins were determined using extinction coefficients at 280 nm, determined from the amino acid sequences. Far-UV CD spectra (190–280 nm, 1-mm path) were collected in 100 mM Na-phosphate, 10 mM Tris-HCl buffer (pH 7.5) at 20 °C on Chirascan (Applied Photophysics) CD spectrophotometer. All reported spectra are averages of three scans; for each, the appropriate baseline (without protein) was subtracted. Protein concentrations in these experiments ranged between 5 and 7 μM. The secondary structure predictions based on the different CD spectra were performed by the CDSSTR algorithm in Dichroweb (48, 49). Fluorescence was collected in a Cary Eclipse spectrofluorimeter (Varian) at 20 °C (1-cm path, excitation at 285 nm; emission probed at 295–500 nm, 10-nm slits) in the same buffer as for the CD experiments (6.5–7.5 μM protein). Excitation at 285 nm results in mostly Trp emission but with some contribution from Tyr residues. Med8 and Med18 each has 3 Trp, Med20 has 2 Trp, Med8 has 4 Tyr, Med18 has 10 Tyr, and Med20 has 5 Tyr.

Urea-induced unfolding of Med8 (7 μM) at 20 °C was probed by CD at 220 nm and fluorescence (λ$_{max}$) as a function of increasing urea (highest grade, from MP Biomedicals) concentrations in 0.5 M increments from 0 to 8 M (30-min incubation time; longer or shorter times did not change the result). Reversibility was tested by dilution experiments from high to low urea concentrations.

1. Conaway RC, Conaway JW (1993) General initiation factors for RNA polymerase II. *Annu Rev Biochem* 62:161–190.
2. Takagi Y, Kornberg RD (2006) Mediator as a general transcription factor. *J Biol Chem* 281:80–89.
3. Björklund S, Gustafsson CM (2005) The yeast Mediator complex and its regulation. *Trends Biochem Sci* 30:240–244.
4. Kornberg RD (2005) Mediator and the mechanism of transcriptional activation, *Trends Biochem Sci* 30:235–239.
5. Conaway RC, Sato S, Tomomori-Sato C, Yao T, Conaway JW (2005) The mammalian Mediator complex and its role in transcriptional regulation. *Trends Biochem Sci* 30:250–255.
6. Fondell JD, Ge H, Roeder RG (1996) Ligand induction of a transcriptionally active thyroid hormone receptor coactivator complex. *Proc Natl Acad Sci USA* 93:8329–8333.

7. Chao DM, et al. (1996) A mammalian SRB protein associated with an RNA polymerase II holoenzyme. *Nature* 380:82–85.
8. Gu JY, et al. (2002) Novel Mediator proteins of the small Mediator complex in *Drosophila* SL2 cells. *J Biol Chem* 277:27154–27161.
9. Jiang YW, et al. (1998) Mammalian mediator of transcriptional regulation and its possible role as an end-point of signal transduction pathways. *Proc Natl Acad Sci USA* 95:8538–8543.
10. Kwon JY, et al. (1999) *Caenorhabditis elegans* mediator complexes are required for developmental-specific transcriptional activation. *Proc Natl Acad Sci USA* 96:14990–14995.
11. Spåhr H, et al. (2000) Purification and characterization of RNA polymerase II holoenzyme from *Schizosaccharomyces pombe*. *J Biol Chem* 275:1351–1356.
12. Bäckström S, Elfving N, Nilsson R, Wingsle G, Björklund S (2007) Purification of a plant mediator from *Arabidopsis thaliana* identifies PFT1 as the Med25 subunit. *Mol Cell* 26:717–729.
13. Kim YJ, Björklund S, Li Y, Sayre MH, Kornberg RD (1994) A multiprotein mediator of transcriptional activation and its interaction with the C-terminal repeat domain of RNA polymerase II. *Cell* 77:599–608.
14. Asturias FJ, Jiang YW, Myers LC, Gustafsson CM, Kornberg RD (1999) Conserved structures of mediator and RNA polymerase II holoenzyme. *Science* 283:985–987.
15. Li Y, et al. (1995) Yeast global transcriptional regulators Sin4 and Rgr1 are components of mediator complex/RNA polymerase II holoenzyme. *Proc Natl Acad Sci USA* 92:10864–10868.
16. Dotson MR, et al. (2000) Structural organization of yeast and mammalian mediator complexes. *Proc Natl Acad Sci USA* 97:14307–14310.
17. Guglielmi B, et al. (2004) A high resolution protein interaction map of the yeast Mediator complex. *Nucleic Acids Res* 32:5379–5391.
18. Lee YC, Kim YJ (1998) Requirement for a functional interaction between mediator components Med6 and Srb4 in RNA polymerase II transcription. *Mol Cell Biol* 18:5364–5370.
19. Nonet ML, Young RA (1989) Intragenic and extragenic suppressors of mutations in the heptapeptide repeat domain of *Saccharomyces cerevisiae* RNA polymerase II. *Genetics* 123:715–724.
20. Takagi Y, et al. (2006) Head module control of mediator interactions. *Mol Cell* 23:355–364.
21. Hoeppner S, Baumli S, Cramer P (2005) Structure of the mediator subunit cyclin C and its implications for CDK8 function. *J Mol Biol* 350:833–842.
22. Koschubs T, et al. (2009) Identification, structure, and functional requirement of the Mediator submodule Med7N/31. *EMBO J* 28:69–80.
23. Larivière L, et al. (2008) Structure-system correlation identifies a gene regulatory Mediator submodule. *Genes Dev* 22:872–877.
24. Baumli S, Hoeppner S, Cramer P (2005) A conserved mediator hinge revealed in the structure of the MED7.MED21 (Med7.Srb7) heterodimer. *J Biol Chem* 280:18171–18178.
25. Larivière L, et al. (2006) Structure and TBP binding of the Mediator head subcomplex Med8-Med18-Med20. *Nat Struct Mol Biol* 13:895–901.
26. Jackson SE (1998) How do small single-domain proteins fold? *Fold Des* 3:R81–R91.
27. Privalov P (1997) Thermodynamics of protein folding. *J Chem Thermodyn* 29:447–474.
28. Fersht A (1999) in *Structure and Mechanism in Protein Science: A Guide to Enzyme Catalysis and Protein Folding* (W.H. Freeman and Company, New York).
29. Jaenicke R, Lilie H (2000) Folding and association of oligomeric and multimeric proteins. *Adv Protein Chem* 53:329–401.
30. Mateu MG, Sanchez Del Pino MM, Fersht AR (1999) Mechanism of folding and assembly of a small tetrameric protein domain from tumor suppressor p53. *Nat Struct Biol* 6:191–198.
31. Chen J, Smith DL (2000) Unfolding and disassembly of the chaperonin GroEL occurs via a tetradecameric intermediate with a folded equatorial domain. *Biochemistry* 39:4250–4258.
32. Luke K, Perham M, Wittung-Stafshede P (2006) Kinetic folding and assembly mechanisms differ for two homologous heptamers. *J Mol Biol* 363:729–742.
33. Tóth-Petróczy A, et al. (2008) Malleable machines in transcription regulation: The mediator complex. *PLoS Comput Biol* 4:e1000243.
34. Johnson WC, Jr (1990) Protein secondary structure and circular dichroism: A practical guide. *Proteins* 7:205–214.
35. Daggett V, Fersht A (2003) The present view of the mechanism of protein folding. *Nat Rev Mol Cell Biol* 4:497–502.
36. Matthews CR (1993) Pathways of protein folding. *Annu Rev Biochem* 62:653–683.
37. Staley JP, Woolford JL, Jr (2009) Assembly of ribosomes and spliceosomes: Complex ribonucleoprotein machines. *Curr Opin Cell Biol* 21:109–118.
38. Williamsson JR (2003) After the ribosome structures: How are the subunits assembled? *RNA* 9:165–167.
39. Kornberg RD (1974) Chromatin structure: A repeating unit of histones and DNA. *Science* 184:868–871.
40. Luger K, Mader AW, Richmond RK, Sargent DF, Richmond TJ (1997) Crystal structure of the nucleosome core particle at 2.8 A resolution. *Nature* 389:251–260.
41. Sogo JM, Stahl H, Koller T, Knippers R (1986) Structure of replicating simian virus 40 minichromosomes. The replication fork, core histone segregation and terminal structures. *J Mol Biol* 189:189–204.
42. English CM, Adkins MW, Carson JJ, Churchill ME, Tyler JK (2006) Structural basis for the histone chaperone activity of Asf1. *Cell* 127:495–508.
43. Arents G, Burlingame RW, Wang BC, Love WE, Moudrianakis EN (1991) The nucleosomal core histone octamer at 3.1 Å resolution: A tripartite protein assembly and a left-handed superhelix. *Proc Natl Acad Sci USA* 88:10148–10152.
44. Xie X, et al. (1996) Structural similarity between TAFs and the heterotetrameric core of the histone octamer. *Nature* 380:316–322.
45. Birck C, et al. (1998) Human TAFII28 and TAFII18 interact through a histone fold encoded by atypical evolutionary conserved motifs also found in the SPT3 family. *Cell* 94:239–249.
46. Gangloff Y-G, et al. (2001) Histone folds mediate selective heterodimerization of yeast TAFII25 with TFIID components yTAFII47 and yTAFII65 and with SAGA component ySPT7. *Mol Cell Biol* 21:1841–1853.
47. Fribourg S, et al. (2001) Dissecting the interaction network of multiprotein complexes by pairwise coexpression of subunits in *E. coli*. *J Mol Biol* 306:363–373.
48. Sreerama N, Woody RW (2000) Estimation of protein secondary structure from circular dichroism spectra: Comparison of CONTIN, SELCON, and CDSSTR methods with an expanded reference set. *Anal Biochem* 287:252–260.
49. Whitmore L, Wallace BA (2008) Protein secondary structure analyses from circular dichroism spectroscopy: Methods and reference databases. *Biopolymers* 89:392–400.

BIOCHEMISTRY